

An experimental study on shear mechanical properties of clay-concrete interface with different roughness of contact surface

Wendong Yang^{*1}, Ling Wang^{1a}, Jingjing Guo^{2b} and Xuguang Chen^{**3}

¹College of Pipeline and Civil Engineering, China University of Petroleum, Qingdao, Shandong, 266580, China

²China Construction Second Engineering Bureau Ltd, Beijing, 100160, China

³College of Engineering, Ocean University of China, Qingdao, Shandong, 266100, China

(Received June 6, 2020, Revised August 27, 2020, Accepted September 7, 2020)

Abstract. In order to understand the shear mechanical properties of the interface between clay and structure and better serve the practical engineering projects, it is critical to conduct shear tests on the clay-structure interface. In this work, the direct shear test of clay-concrete slab with different joint roughness coefficient (JRC) of the interface and different normal stress is performed in the laboratory. Our experimental results show that (1) shear strength of the interface between clay and structure is greatly affected by the change of normal stress under the same condition of JRC and shear stress of the interface gradually increases with increasing normal stress; (2) there is a critical value JRC_{cr} in the roughness coefficient of the interface; (3) the relationship between shear strength and normal stress can be described by the Mohr Coulomb failure criterion, and the cohesion and friction angle of the interface under different roughness conditions can be calculated accordingly. We find that there also exists a critical value JRC_{cr} for cohesion and the cohesion of the interface increases first and then decreases as JRC increases. Moreover, the friction angle of the interface fluctuates with the change of JRC and it is always smaller than the internal friction angle of clay used in this experiment; (4) the failure type of the interface of the clay-concrete slab is type I sliding failure and does not change with varying JRC when the normal stress is small enough. When the normal stress increases to a certain extent, the failure type of the interface will gradually change from shear failure to type II sliding failure with the increment of JRC.

Keywords: JRC; shear test; clay-concrete interface; shear strength; cohesion; friction angle

1. Introduction

The interaction between soil and structure is always an important research topic in the fields of civil engineering and geotechnical engineering. Mechanical properties of the soil-structure interface are important factors that affect the bearing capacity of the building or structure, and the roughness of the structure also has a strong influence on the mechanical properties of the interface. Therefore, understanding the shear performance of the soil-structure interface is paramount for the correct evaluation of the construction quality, ensuring construction safety, and the reasonable reduction of the engineering cost, which has very important theoretical research significance and engineering practical value.

Many scholars have conducted shear tests on the soil-structure interface to study different factors affecting the shear performance of the interface. Mortara (2007) conducted shear tests by using an improved direct shear apparatus (that is, the constant normal stiffness direct shear

apparatus,) to study the friction characteristics of the interface and soil deformability. Zhang and Zhang (2006, 2009) believed that the three factors that had the greatest influence on the mechanical behavior of the interface were the size of coarse-grained soil particle, the roughness of the contact surface, and the normal stress by carrying out monotonic cyclic shear tests on the interface of coarse-grained soil and structure. Aksoy *et al.* (2016) added different ratios of low plastic clay into the sand to obtain sand with different friction angle. The friction angle between the sand and different material structures was measured through the interface shear test, which provided the basis for the pile design in the actual project. Hu and Pu (2004) conducted a series of direct shear tests on the soil-structure interface and they found that there was a critical roughness value on the soil-structure interface, and the failure mode can be divided into shear failure and sliding failure according to the different roughness. Zhang *et al.* (2006) observed and measured the movement of soil particles in the soil-structure interface tests by using a new micro measurement method, and the results showed that the roughness and normal stress of the interface had a very significant effect on the movement of soil particles near the structure. Canakci *et al.* (2016) conducted direct shear tests on the contact surface of soil with concrete, steel, wood and other building materials under different normal stresses, and they believed that the water content of soil, the type of material and the roughness of the contact surface had a great impact on the friction characteristics between building

*Corresponding author, Ph.D.

E-mail: yangwd@upc.edu.cn

**Corresponding author, Ph.D.

E-mail: chenxuguang1984@ouc.edu.cn

^aPh.D. Student

E-mail: 1499892715@qq.com

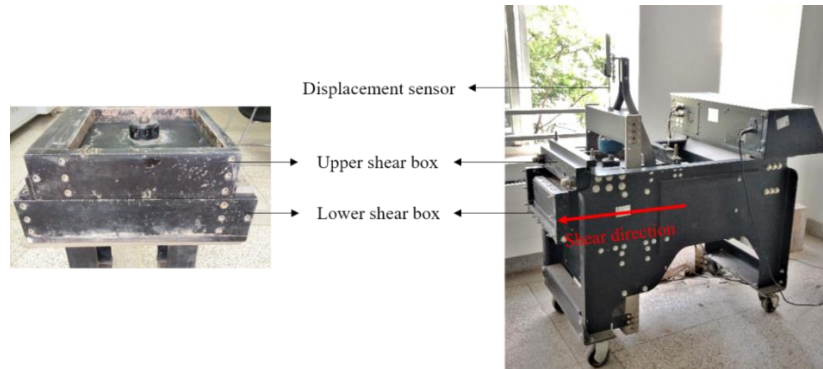


Fig. 1 ShearTrac III direct shear apparatus

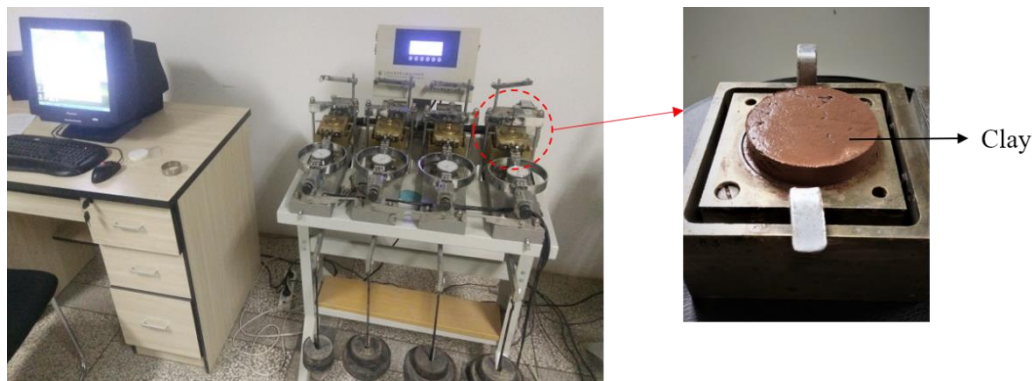


Fig. 2 ZJ type strain controlled direct shear apparatus (quadruple shear) and clay sample

materials and soil. Samanta *et al.* (2018) analyzed the interface shear strength of sand and different building materials, namely steel and concrete, by using direct shear test device, and studied the influence of surface roughness, average grain size of sand particles, relative density of sand body and size of direct shear box on the interface shear performance of sand, steel and concrete. Mu *et al.* (2019) established a slurry diffusion model for single random rough fracture considering the coupling effect of slurry and geological fracture, studied the flow characteristics and coupling response of slurry in the rough fracture, and claimed that the roughness and shear stress between the cracks were the main factors causing the grouting split. Gu *et al.* (2017) and Huang *et al.* (2019) used the discrete element method to study the cyclic shear behavior of soil structure interface at the macro and micro levels. Saberi *et al.* (2016, 2018, 2019) proposed different plastic constitutive models to solve the shear behavior of soil structure interface, and studied the stress characteristics between gravel soil, sand soil and structure interface. Jing *et al.* (2017) performed a series of three-dimensional interface shear tests using the discrete element method with various degrees of normalized roughness and analyzed the effect of roughness on the shearing behavior of the soil-hard structure interface. Moreover, several researchers (Feng *et al.* 2012, Su *et al.* 2018) carried out a series of monotonic direct shear tests on the interface between coarse-grained soil and steel, and studied the influence of the relative roughness and average particle size of coarse-grained soil on the shear behavior of the interface between sand and steel. Farhadi (2017) and Lashkari (2010) conducted a

series of extensive direct shear tests to study the shear mechanical properties of the sand-structure interface, and proposed an interface model based on the generalized plastic theory to describe the effect of cyclic rotational shear on the mechanical behavior of the sand-structure interfaces. The influence of temperature on the physical and mechanical properties of soil-structure interface has also been studied by many scholars (Di Donna *et al.* 2016, Zhao *et al.* 2017, Yazdani *et al.* 2019, Xiao *et al.* 2014).

In the studies mentioned above, the contact surfaces of different types of soil and structure were tested. However, the shear mechanical properties between clay and structure have been rarely studied. The study of friction angle and cohesion in contact surface under different surface roughness and normal stress is limited. In this paper, we explore the relationship between shear strength and shear displacement of the interface and investigate shear deformation characteristics under different normal stress and roughness through direct shear tests of the clay-concrete slab with different roughness coefficients. Furthermore, Mohr Coulomb criterion is used to describe the relationship between shear strength and normal stress of the interface to study the influence of roughness coefficient of interface on cohesion and friction angle, and the failure mechanism of contact surface.

2. Laboratory test

2.1 Experimental preparation

Fig. 1 shows the large-scale direct shear apparatus

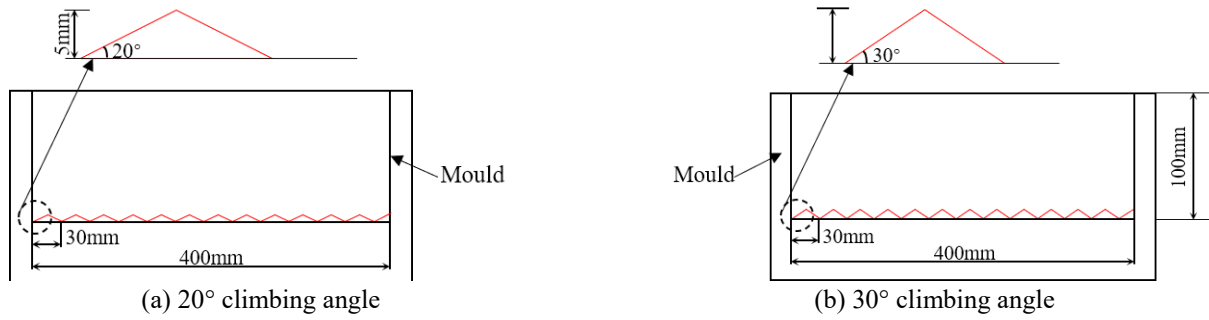


Fig. 3 Schematic diagram of sawtooth concrete mould



(a) Group A - 0° climbing angle concrete slab (b) Group B - 20° climbing angle concrete slab (c) Group C - 30° climbing angle concrete slab

Fig. 4 The finished concrete slab with regular sawtooth



Fig. 5 Splitting test of the concrete slab



(a) Group D

(b) Group E

(c) Group F

Fig. 6 Concrete slab with random roughness after splitting

(model: ShearTrac III) used in this study. The sample size in the testing apparatus is $305 \times 305 \times 100$ mm (length \times width \times height) for the upper shear box and $400 \times 305 \times 100$ mm for the lower shear box. The maximum horizontal load of the direct shear apparatus can be up to 50 kN, and the horizontal load can be applied at a constant displacement rate up to 15 mm/min.

2.2 Specimen preparation

Clay samples are recovered from a coastal oil storage project in this work. The shear strength parameters of the field clay in the engineering geological exploration report are taken as the basis when preparing the sample. The shear strength parameters of samples with different water

contents are measured first because the shear strength of clay samples is largely affected by the moisture content. The clay samples with different moisture contents are made respectively. The values of cohesion and internal friction angle of these samples are determined by carrying out quick consolidated shear tests with ZJ type strain controlled direct shear apparatus (quadruple shear). Fig. 2 shows the ZJ type strain controlled direct shear apparatus (quadruple shear) and clay sample. Experimental results show that the moisture content of the clay is 20%, the cohesion is 40.86 kPa, and internal friction angle is 22°. The clay samples in the follow-up tests are all made by using this parameter ratio.

In this work, the preparation process of the soil sample is strictly controlled as a very important part. The soil used in the test is silty clay with natural saturated moisture content of 33.9%, liquid limit of 32.8%, plastic limit of 17.5% and plasticity index of 15.3. There is no organic matter in the soil. The clay with the same proportion of parameters mentioned above is added to the upper shear box by layer method after the soil sample is sealed and consolidated, and there are five layers in total. The weight of the first three layers of soil samples is the same, which is 2 kg. After weighing the required weight of clay, put it into the upper shear box and make it evenly distributed as far as possible. After that, the soil sample is compacted by light compaction test, and each tamping hit is hit 56 times. And then the upper surface of the clay is then roughened with a scraper to bond more tightly with the clay above. The last two layers of soil samples each weigh 1.5 kg. The fourth layer of soil sample is compacted and roughened with the same method mentioned above. For the fifth layer of soil sample, it is only necessary to tamp them without scratching the upper surface.

The testing program is divided into 6 groups according to different roughness of concrete slab, including 3 groups of regular sawtooth concrete slab and the surface roughness is changed by adjusting the climbing angle of concrete surface sawtooth, which is separately 0°, 20°, 30°. The concrete slab fabrication steps are as follows: (1) weigh cement, sand and water according to the mix proportion of 1:2.34:0.41 by weight; (2) pour the weighed cement and sand into the mixer, fully mix and add the corresponding weight of water, and then mix for 5 to 10 minutes; (3) fix the triangular prism with fixed angle tightly at the bottom of the formwork to make the concrete slab. (see Fig. 3 for the schematic diagram of the formwork with angle); (4) pour the mixed cement mortar into the formwork, and use the method of layered pouring to ensure the quality of the sample and improve its compactness; (5) place the poured specimens on the vibration table to vibrate until there is no bubble from the surface of the sample; (6) after vibration place the sample under normal temperature, and remove the formwork after 24 hours of mortar hardening; and (7) the test piece is placed in the normal temperature environment for maintenance after the formwork is removed, and the water is sprinkled regularly for 28 days for maintenance. The finished concrete slab is shown in Fig. 4, and their dimensions are listed in Table 1.

There are three other groups of concrete slabs with

Table 1 Dimensions of concrete slab with sawtooth climbing angle

Group	Climbing angle size	Dimensions
A	0°	400 mm×300 mm×100 mm
B	20°	400 mm×300 mm×100 mm
C	30°	400 mm×300 mm×100 mm

Table 2 Dimensions of concrete slab with random roughness surface

Group	Surface roughness category	Dimensions
D	Random rough surface	300 mm×300 mm×75 mm
E	Random rough surface	300 mm×300 mm×75 mm
F	Random rough surface	300 mm×300 mm×75 mm

random roughness. They are two concrete slabs of the same size with irregular surface obtained by splitting test with a large concrete block of 300 × 150 × 150 mm (length × width × height). And the manufacturing process of the random roughness concrete slab is the same as that of the regular sawtooth concrete slab, except that the mould needs to be replaced with the size of 300 × 150 × 150 mm (length × width × height). Because the size of the random roughness concrete slab is not the same as that of the apparatus, two concrete test blocks with the sizes of 400 × 300 × 25 mm (length × width × height) and 100 × 300 × 50 mm (length × width × height) need to be made as cushion blocks to ensure that the position of the concrete slab in the lower shear box is fixed. The splitting test is conducted on a uniaxial compression testing machine and the concrete splitting process is shown in Fig. 5. In order to ensure that the size of the two concrete test blocks obtained by splitting is the same, the central axis of the complete concrete block must be aligned with the upper and lower cushion strips of the splitting fixture, and the testing machine should be controlled to press the fixture at a certain rate until the complete concrete block is cracked. The three groups of random roughness concrete slabs after splitting are shown in Fig. 6, and their dimensions are listed in Table 2.

2.3 Calculation of JRC on rough surface of concrete slab

It is necessary to carry out quantitative analysis on the morphology characteristics of each contact surface for analyzing the influence of surface roughness on the mechanical properties of the interface. In 1973, Barton and Choubey (1977) first proposed ten classical joint contour lines to evaluate the roughness coefficients. According to this method, the roughness value of the structural surface is determined by comparing with the standard profile line, but the error of this method is relatively large because of its strong subjectivity. After many extensive researches, it is found that the surface of rough structural surface can be regarded as many irregular geometric surfaces, so it can be described by statistical parameters or functions. The parameters describing the joint surface morphology can be

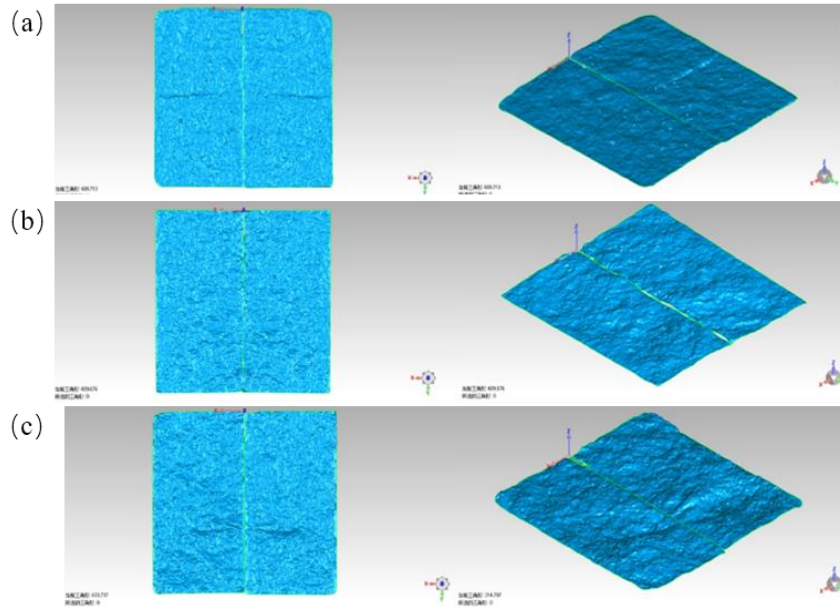


Fig. 7 Joint surface morphology of concrete slab with random roughness (a: Group D; b: Group E; c: Group F)

Table 3 Calculated JRC value of roughness surface for each group of concrete slab

Group	Climbing angle	JRC
A	0°	0
B	20°	16.7079
C	30°	24.9966
D	-	7.3374
E	-	10.5657
F	-	15.0117

divided into two categories: height difference parameter (Lukyanov and Lisenko 1982) and texture parameter (Adler and Firman 1981). Theoretically, the full height distribution density function and autocorrelation function of the surface morphology can describe the geometric characteristics of the surface morphology completely. But in practical application, several parameters or their combinations will be selected according to different purposes.

The characteristic parameters of the height distribution of the surface morphology are also expressed by the correlation moments of the density function of the height distribution, such as the average height of the center line, the root mean square of the height, etc. At the same time, it needs to describe the texture parameters of the surface morphology, such as the forward and reverse shape difference coefficient (Thomas 1981), the frequency spectral density function of the surface morphology (Nayak 1973), and the surface structure function (Sayles and Thomas 1977). In this work, the calculation equation of JRC and the root mean square of slope Z_2 proposed by Tse and Cruden (1979), which are widely used, are selected to calculate the JRC value as,

$$JRC = 32.2 + 32.47lgZ_2 \quad (1)$$

And the Z_2 is obtained by the following formula,

$$Z_2 = \sqrt{\frac{1}{L} \int_0^L \left(\frac{dZ}{dx} \right)^2 dx} \quad (2)$$

where L is the sample length and $Z(x)$ is the random surface profile function.

Eq. (1) is only used for the calculation of a single section line, so the average JRC of the joint surface is used to quantify the morphological characteristics of the rough structure surface in this paper, and the calculation equation can be expressed as,

$$JRC = \frac{1}{m} \sum_{i=1}^m JRC_i \quad (3)$$

where m is the number of profile lines, and JRC_i is the roughness coefficient of the i th profile line.

Eq. (3) can be directly used to calculate the roughness coefficient of regular sawtooth concrete slab. For the random roughness concrete slab, the rough surface of two concrete slabs (length \times width \times height: 300 \times 150 \times 75mm) obtained by splitting is placed upward, the three-dimensional laser scanner is used to collect the roughness information of the structural surface, and then the GEOMAGIC and other relevant software are used to optimize and process the collected structural surface morphology information. Finally, the information of structural surface along the undulating direction of the joint surface is calculated by MATLAB, and the corresponding surface roughness coefficient is obtained. Fig. 7 shows the morphology of the collected random rough surface concrete slab, and the calculated JRC value for each concrete slab is provided in Table 3.

2.4 Experimental design

In the direct shearing tests, the shearing displacement speed is taken as 0.8 mm/min and remains unchanged throughout the shearing process until the specimen is

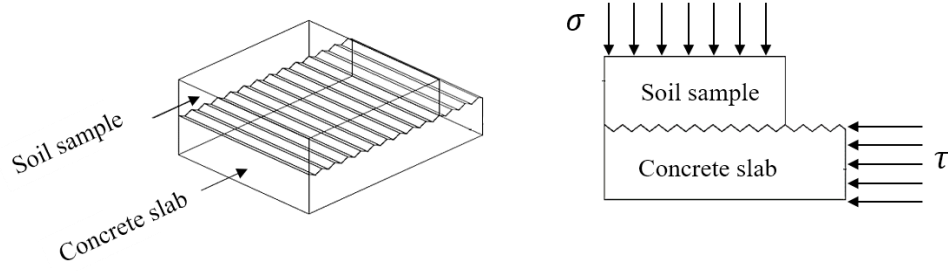


Fig. 8 Diagram of sample placement of consolidated clay-concrete slab and the load application directions

damaged. The normal stress is taken as 100 kPa, 200 kPa, and 400 kPa, respectively. Taking regular sawtooth concrete slab as an example, the diagram of clay sample and concrete slab after consolidation in the direct shear apparatus and the application directions of normal stress and horizontal shear stress are shown in Fig. 8.

3. Experimental results

Fig. 9 shows the initial shear strength-displacement data of each group of clay-concrete slab interface, and the statistical table of initial shear stress is listed in Table 4.

It is worth noting that there is a size difference between the concrete slabs in groups A, B, C, and the concrete slabs in group D, E, F, therefore the error caused by size difference should be considered (Yu *et al.* 2014, Zhang and Wang 2017). In order to eliminate the influence of the change in the actual shear area on the test results in the process of direct shear test, Zhang *et al.* (2017) established a modifier equation based on the shear strength of circular shear box. In this paper, the same calculation method is used to calculate the shear strength modifier equation of rectangular shear box. The calculation equation of shear stress in direct shear test may be written as,

$$\tau_0 = \frac{CR}{S} \quad (4)$$

where S is the initial shear area; C and R are the rigid coefficient and dial indicator readings, respectively.

The initial shear area of the rectangular shear box can be given as,

$$S = \lambda l^2 \quad (5)$$

where l is the side length parallel to the shear direction; λ is the ratio between the side length perpendicular to the shear direction to l .

The effective contact area between the soil sample and the concrete slab after the shear test is started can be expressed as,

$$S_{Actual} = \lambda l(l - \delta) \quad (6)$$

where δ is shear displacement.

The actual shear strength should be:

$$\tau_{Actual} = \frac{CR}{S_{Actual}} \quad (7)$$

The relative error between the initial shear strength and

Table 4 Statistical table of initial peak shear strength

Group	Peak Shear strength τ /kPa		
	100 kPa	200 kPa	400 kPa
A	40.51	70.82	116.72
B	81.87	99.62	161.04
C	67.81	84.47	139.40
D	83.95	108.43	158.16
E	92.70	132.48	166.85
F	86.31	110.72	158.48

Table 5 Statistical table of peak shear strength after correction

Group	Peak Shear strength τ / kPa		
	100 kPa	200 kPa	400 kPa
A	40.51	70.82	116.72
B	81.87	99.62	161.04
C	67.81	84.47	139.40
D	95.14	122.85	179.17
E	105.06	150.05	189.03
F	97.82	125.42	179.51

Table 6 Statistical table of shear failure types

Group	Failure type		
	100 kPa	200 kPa	400 kPa
A	sliding failure	shear failure	shear failure
B	sliding failure	sliding failure	sliding failure
C	sliding failure	sliding failure	sliding failure
D	sliding failure	sliding failure	shear failure
E	sliding failure	sliding failure	shear failure
F	sliding failure	sliding failure	sliding failure

the actual shear strength obtained from the combination of Eqs. (4)-(7) is:

$$e_r = -\frac{\delta}{l} \quad (8)$$

In this work, the maximum shear displacement is 4 cm and the side length parallel to the shear direction is 30 cm. According to Eq. (8), the relative error is 13.33%. The test results of groups D, E and F are corrected according to the

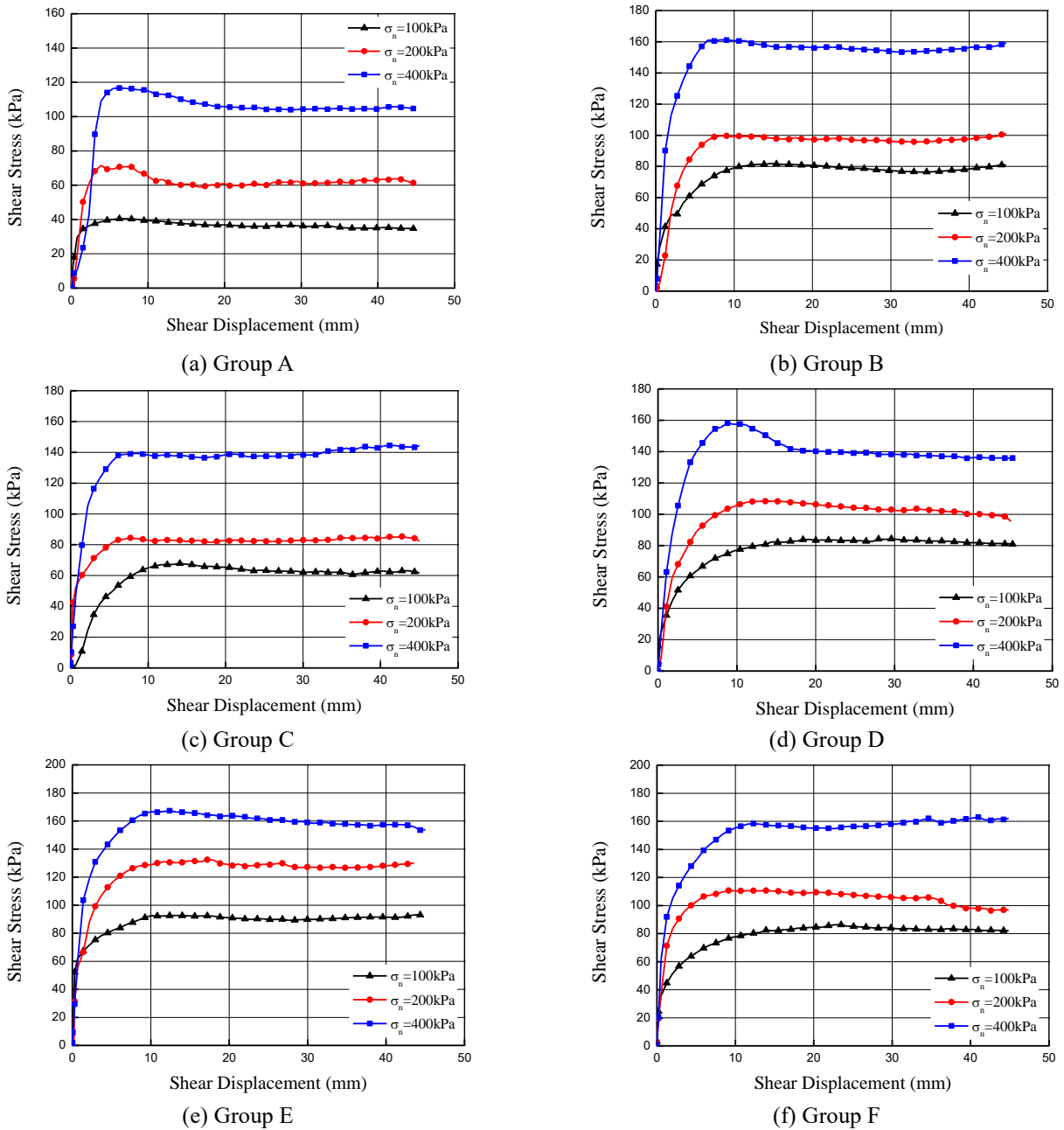


Fig. 9 Initial shear strength-displacement data of contact surface for each group of clay-concrete slab

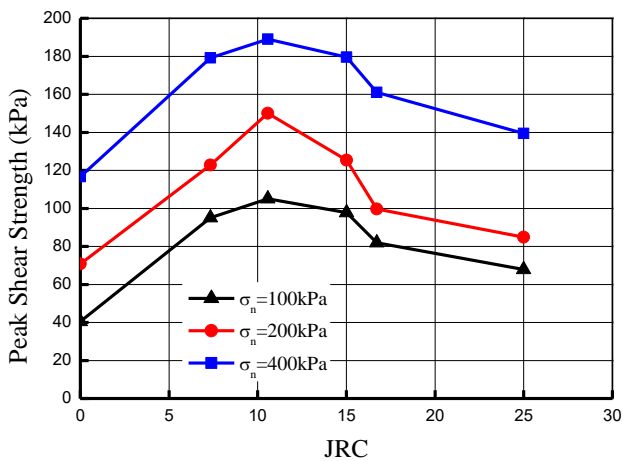


Fig. 10 JRC -peak shear strength curves of contact surfaces

relative error. The corrected results are given in Table 5. Fig. 10 shows the diagram of JRC-peak shear strength under different normal stresses.

The failure types of contact surface can be divided into two categories: shear failure and sliding failure. Based on whether there is obvious peak in the shear strength-displacement curve of each group in Fig. 9 and the failure form of contact surface after the failure of the sample, we can judge the failure type of contact surface for each sample, as shown in Table 6.

The following conclusions may be drawn from Figs. 9-10 and Table 6.

1. When the value of JRC is unchanged, the shear strength of the contact surface of clay-concrete slab is greatly affected by the change of normal stress. Specifically,

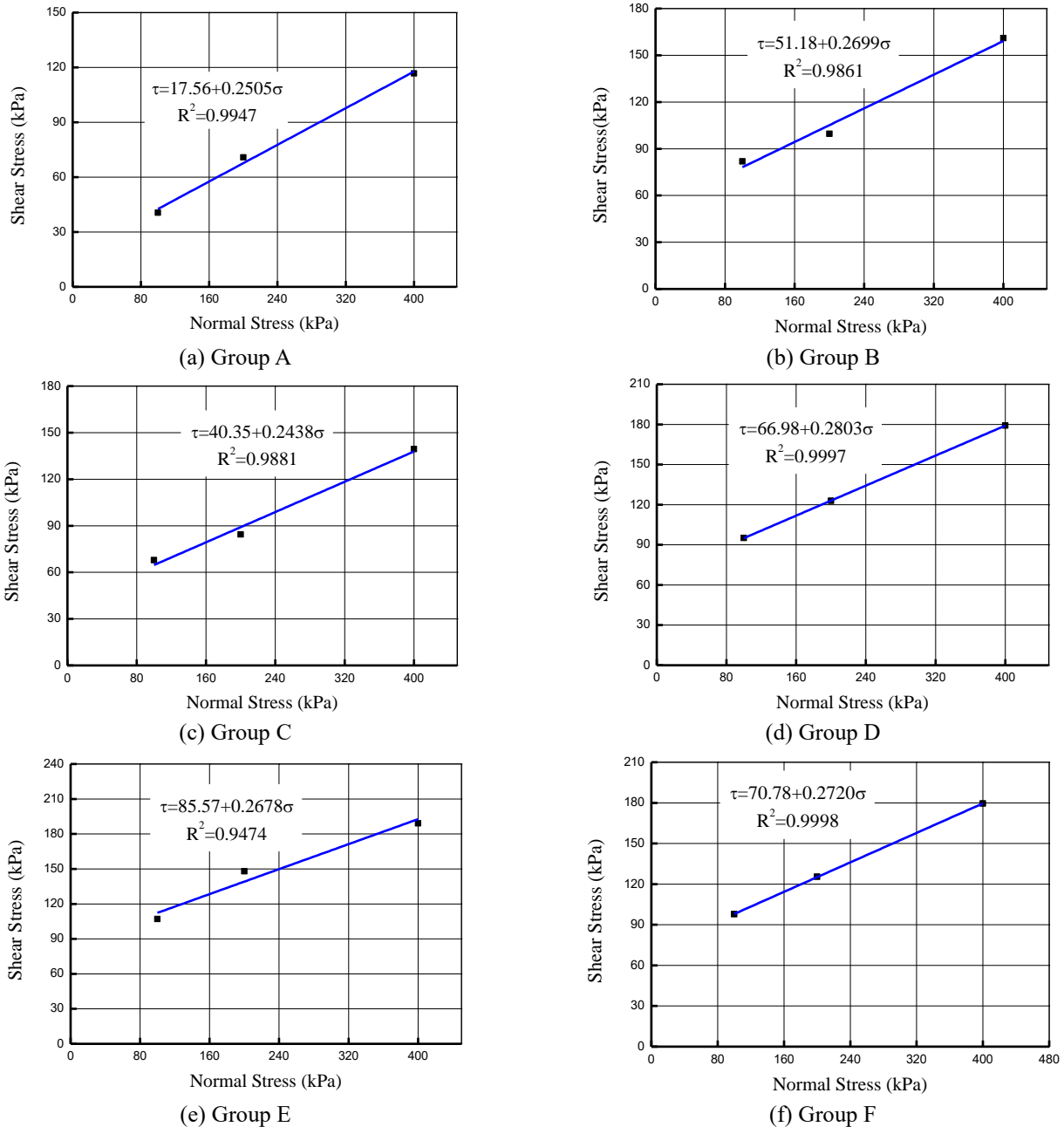


Fig. 11 Fitting curve of shear failure strength of the interface for each group of clay-concrete slab

the shear strength of the interface increases with the increase of normal stress.

2. From the JRC value of rough surface for each group of concrete slab in Table 3, it can be seen that the order of JRC value of each group is: $A < D < E < F < B < C$. From Fig. 10 we find that under the same normal stress, the shear strength of contact surface increases first and then decreases with the increase of JRC, which indicates that there is a critical value JRC_{cr} for joint roughness coefficient. Under the condition of constant normal stress, the shear strength of contact surface increases with the increase of JRC when $JRC < JRC_{cr}$; while the shear strength of contact surface decreases with the increase of JRC when $JRC \geq JRC_{cr}$.

3. We observe that the failure type of all clay-concrete interfaces is sliding failure when the normal stress is 100

kPa. When the normal stress is 200 kPa, the failure type of group A is shear failure, but it is sliding failure in group B, C, D, E and F. When the normal stress is 400 kPa, the failure type of group A, D and E is shear failure, while it is sliding failure in group F, B and C, which means that the failure type of contact surface gradually changes from shear failure to sliding failure with the increase of JRC.

4. Discussions

4.1 Analysis of mechanical properties of clay-concrete interface

The relationship between peak shear strength and normal stress of clay-concrete interface is shown in Fig. 11

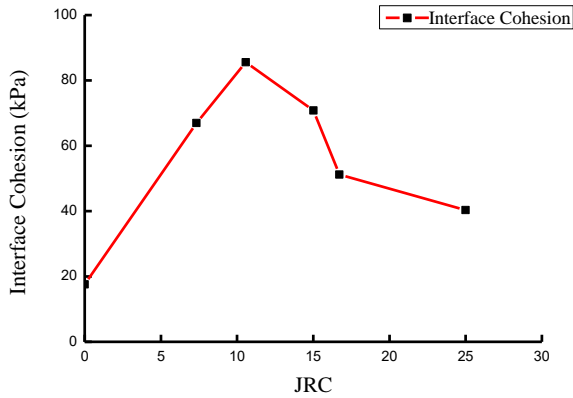


Fig. 12 The relationship between the interface cohesion and JRC

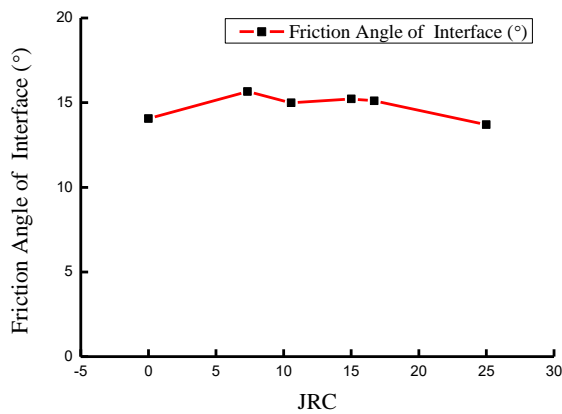


Fig. 13 The relationship between the friction angle of interface and JRC

Table 7 Statistical table of shear strength parameters

Group	Fitting equation	Cohesion c /kPa	Friction angle φ /°	correlation coefficient R^2
A	$\tau = 17.56 + 0.2505 \sigma$	17.56	14.06	0.9947
B	$\tau = 51.18 + 0.2699 \sigma$	51.58	15.10	0.9861
C	$\tau = 40.35 + 0.2438 \sigma$	40.35	13.70	0.9881
D	$\tau = 66.98 + 0.2803 \sigma$	66.98	15.66	0.9997
E	$\tau = 85.57 + 0.2678 \sigma$	85.57	14.99	0.9474
F	$\tau = 70.78 + 0.2720 \sigma$	70.78	15.22	1.0000

based on the data in Table 5. We find that the relationship between them conforms to the Mohr Coulomb failure criterion. Therefore, Mohr Coulomb failure criterion is used to calculate the cohesion and the friction angle of the interface:

$$\tau = \sigma \tan \varphi + c \quad (9)$$

where τ is the shear stress of the interface, and σ is the normal stress.

The shear strength parameters of each group obtained by the Mohr Coulomb failure criterion are listed in Table 7. Fig. 12 shows the relationship between the cohesion of the interface and JRC. We find that the cohesion of clay-concrete slab interface increases first and then decreases as

JRC increments. This shows that there is also a critical roughness coefficient JRC_{cr} for the cohesion of the interface. The cohesion of the contact surface will increase as the roughness coefficient of the contact surface increases when $JRC < JRC_{cr}$; while the cohesion will decrease with the increase of the roughness coefficient when $JRC \geq JRC_{cr}$. Theoretically, the cohesion will fluctuate around the cohesion of the clay itself when JRC decreases to a certain extent.

In order to study the influence of the roughness coefficient of the contact surface on the friction angle, the relationship curve between them is shown in Fig. 13. As expected, we find that the friction angle of each interface is smaller than the friction angle of clay itself. Moreover, it is found that the friction angle of the interface of clay-concrete slab varies with the roughness within a small range. The reason for this phenomenon is that the shear stress at the contact surface of clay and concrete slab is relatively complex, including the binding force between clay and concrete slab surface, the relative movement between the clay on the rough part of the contact surface and the upper soil mass, and the friction force between clay and concrete structure surface. And the action mechanism of normal stress on these shear stresses is different, so the change of friction angle has no obvious regularity, but fluctuates in a small range.

4.2 Analysis of failure mechanism of clay-concrete slab interface

According to previous research experience, the failure types of soil-structure interface can be categorized as shear failure and sliding failure, as described as follows. (1) In general, when the normal stress is relatively small, the failure will occur on the interface of clay-concrete slab when the sliding failure occurs. The failure is mainly related to the sliding clay particles on the surface of the concrete slab. The upper soil sample is not damaged when the failure occurs. We name this failure type as type I sliding failure. (2) However, the failure type of the contact surface is still sliding failure when the normal stress increases to a certain extent, but the upper soil sample has been damaged and formed its own damaged zone at this time, and its failure is mainly related to the internal shear deformation of the soil. We call this failure type as type II sliding failure. (3) The failure surface formed by shearing is on the clay-concrete slab interface when the failure type is shear failure, this type of failure is related to the sliding clay particles on the concrete slab surface and the internal shear deformation of the upper soil mass.

As listed in Table 6, the failure type of the interface of clay-concrete slab is sliding failure when the normal stress is 100 kPa and the failure mode will not change with the change of the JRC of the contact surface. This is because when the normal stress is small, the failure of the contact surface is mainly controlled by the clay sliding particles on the surface of the concrete slab. The shear strength is primarily provided by the friction between the concrete slab and the upper clay particles. When the JRC of the joint surface of the concrete slab is less than the critical value, the friction between the concrete slab and the upper clay

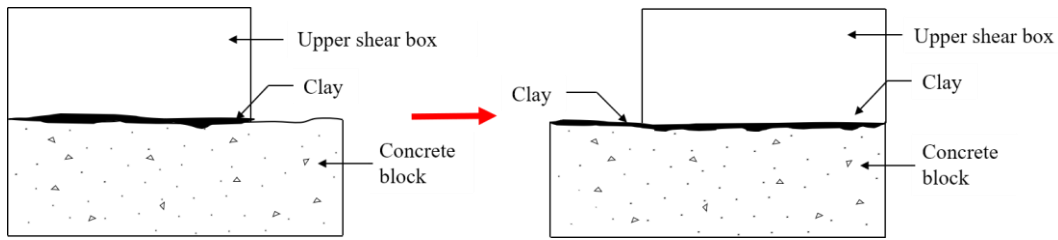


Fig. 14 Schematic diagram of shearing process of type I sliding failure

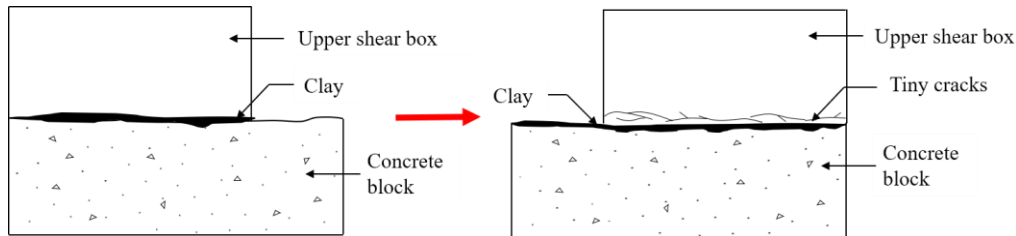


Fig. 15 Schematic diagram of shearing process of shear failure

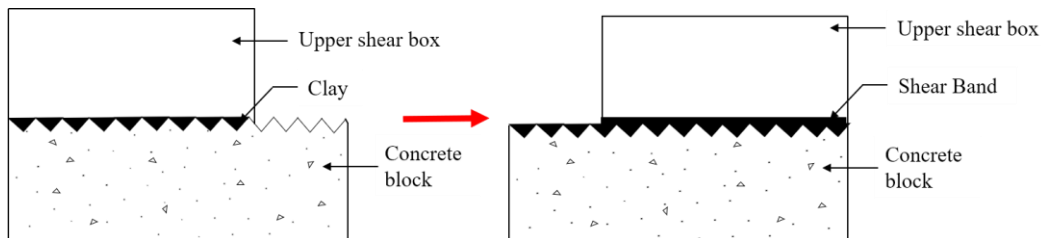


Fig. 16 Schematic diagram of shearing process of type II sliding failure

sample will increase as JRC increases, so the shear strength of the contact surface will increase. However, when the joint surface JRC of the concrete slab is larger than this critical value, the accumulated clay particles on the surface of the concrete slab will increase with increasing JRC, and the friction force between the clay specimen and the concrete slab will decrease as shear progresses, so the shear strength of the contact surface will decrease. Fig. 14 shows the shear process of type I sliding failure of clay-concrete slab interface.

When the normal stress is 400 kPa, it is found that the failure type of contact surface in group A, D and E is shear failure, while that in group F, B and C is sliding failure with the increase of JRC, which means that the failure type gradually changes from shear failure to type II sliding failure as JRC increases. We first discuss the shear failure in three groups of tests as follows. In these direct shearing tests, the shear strength of the contact surface is mainly determined by the friction between clay particles and concrete slab at first, while as shearing continues, the shear strength is then contributed by the friction between the clay particles and the concrete slab surface and the strength of the upper soil itself. When the shear displacement reaches a certain value, the shear strength of the contact surface reaches the maximum value. At this time, the shear failure surface is formed between clay and concrete slab. Fig. 15 shows the schematic of the shearing process clay-concrete slab interface where shear failure is shown on the right figure. Secondly, we explain the other three groups of tests, in which the failure type of contact surface is sliding failure.

With increasing JRC and over a certain critical value, the failure type of the specimen changes from shear failure to type II sliding failure. This is because the surface roughness of the concrete slab is large and the upper soil quickly forms its own shearing damaged zone. In this case, the shear strength of contact surface is mainly controlled by the shear strength of the soil itself. Fig. 16 shows a schematic of the shearing process of type II sliding failure of clay-concrete slab interface.

5. Conclusions

In this paper, we conducted direct shearing tests on clay-concrete with different contact surface roughness and obtained the relationship between shear strength and shear displacement of the contact surface. The relationship between shear strength and normal stress of the contact surface with different roughness is well fitted by the Mohr Coulomb failure criterion. The influence of JRC on the shear strength and other mechanical properties of the interface between clay and concrete slab is studied, and the formation mechanism of shear failure surface is analyzed. The following conclusions may be drawn from this study.

- Under the condition of constant JRC, the shear strength of the contact surface of clay-concrete is greatly affected by the change of normal stress, which shows that the peak value of shear strength increases with increasing normal stress.
- There exists a critical value JRC_{cr} for the joint surface roughness of concrete. Under the condition of constant

normal stress, the shear strength of interface increases with the increase of JRC when $JRC < JRC_{cr}$; while the shear strength decreases with the increase of JRC when $JRC \geq JRC_{cr}$. Theoretically, the shear strength of the contact surface should be reduced to the shear strength of the clay itself and become stable.

- The relationship between peak shear strength of clay-concrete slab interface and normal stress can be described by the Mohr Coulomb failure criterion. The cohesion and friction angle of the contact surface under different roughness are calculated according to the Mohr Coulomb criterion. There is also a critical value JRC_{cr} for the cohesion of the clay-concrete interface. The cohesion increases with the increase of JRC when $JRC < JRC_{cr}$; while the cohesion decreases with the increase of JRC when $JRC \geq JRC_{cr}$. Furthermore, in theory, the cohesion should reach a stable value near the cohesion of clay itself. The change of JRC on the joint surface of concrete slab has no obvious effect on the friction angle of the interface. The friction angle only fluctuates within a small range and is always smaller than the internal friction angle of clay itself.

- The failure type of the interface of the clay-concrete slab is type I sliding failure when the normal stress is relatively small, and the failure type will not change with the JRC change and the upper clay specimen is not damaged. The failure type of contact surface will gradually change from shear failure to type II sliding failure with the increase of JRC when the normal stress increases to a certain extent, and the upper clay sample will have different degrees of failure.

Acknowledgments

The authors gratefully acknowledge the financial support of the National Science Foundation of China under Grant No. 51979281. This work is also supported by the Natural Science Foundation of Shandong Province China No. ZR2018MEE050, and the Fundamental Research Funds for the Central Universities No. 18CX02079A.

References

- Adler, R.J. and Firman, D. (1981), "A non-gaussian model for random surfaces", *Philos. Trans. R. Soc. London Ser. Math. Phys. Sci.*, **303**(1479), 433-462. <https://doi.org/10.1098/rsta.1981.0214>.
- Aksoy, H.S., Gor, M. and Inal, E. (2016), "A new design chart for estimating friction angle between soil and pile materials", *Geomech. Eng.*, **10**(3), 315-324. <https://doi.org/10.12989/gae.2016.10.3.315>.
- Barton, N. and Choubey, V. (1977), "The shear strength of rock joints in theory and practice", *Rock Mech.*, **10**(1-2), 1-54. <https://doi.org/10.1007/BF01261801>.
- Barton, N. and Choubey, V. (1977), "The shear strength of rock joints in theory and practice", *Rock Mech. Felsmech. Mec. Roches.*, **10**, 1-54. <https://doi.org/10.1007/BF01261801>.
- Canakci, H., Hamed, M., Celik, F., Sidik, W. and Eviz, F. (2016), "Friction characteristics of organic soil with construction materials", *Soils Found.*, **56**(6), 965-972. <https://doi.org/10.1016/j.sandf.2016.11.002>.
- Di Donna, A., Ferrari, A. and Laloui, L. (2016), "Experimental investigations of the soil-concrete interface: Physical mechanisms, cyclic mobilization, and behaviour at different temperatures", *Can. Geotech. J.*, **53**(4), 659-672. <https://doi.org/10.1139/cgj-2015-0294>.
- Farhadi, B. and Lashkari, A. (2017), "Influence of soil inherent anisotropy on behavior of crushed sand-steel interfaces", *Soils Found.*, **57**(1), 111-125. <https://doi.org/10.1016/j.sandf.2017.01.008>.
- Feng, D., Hou, W. and Zhang, J. (2012), "Large-scale direct shear test investigation of the 3D behavior of a gravel-structure interfaces", *China Civ. Eng. J.*, **45**(5), 169-175.
- Gu, X., Chen, Y. and Huang, M. (2017), "Critical state shear behavior of the soil-structure interface determined by discrete element modeling", *Particuology*, **35**, 68-77. <https://doi.org/10.1016/j.partic.2017.02.002>.
- Hu, L. and Pu, J. (2004), "Testing and modeling of soil-structure interface", *J. Geotech. Geoenviron. Eng.*, **130**(8), 851-860. [https://doi.org/10.1061/\(ASCE\)1090-0241\(2004\)130:8\(851\)](https://doi.org/10.1061/(ASCE)1090-0241(2004)130:8(851)).
- Huang, M., Chen, Y. and Gu, X. (2019), "Discrete element modeling of soil-structure interface behavior under cyclic loading", *Comput. Geotech.*, **107**, 14-24. <https://doi.org/10.1016/j.compgeo.2018.11.022>.
- Jing, X., Zhou, W. and Li, Y. (2017), "Interface direct shearing behavior between soil and saw-tooth surfaces by DEM simulation", *Proc. Eng.*, **175**, 36-42. <https://doi.org/10.1016/j.proeng.2017.01.011>.
- Kai, Y., Xin, Y. and Yongshuang, Z. (2014), "Analysis of direct shear test data based on area and stress correction", *Chin. J. Rock Mech. Eng.*, **33**(1), 118-124.
- Lashkari, A. (2010), "Modeling of sand-structure interfaces under rotational shear", *Mech. Res. Commun.*, **37**(1), 32-37. <https://doi.org/10.1016/j.mechrescom.2009.09.005>.
- Lashkari, A. (2017), "A simple critical state interface model and its application in prediction of shaft resistance of non-displacement piles in sand", *Comput. Geotech.*, **88**, 95-110. <https://doi.org/10.1016/j.compgeo.2017.03.008>.
- Lukyanov, V.S. and Lisenko, V.G. (1982), "The measurement of surface topography parameters described by the composition of the random and deterministic components", *Wear*, **83**(1), 79-89. [https://doi.org/10.1016/0043-1648\(82\)90342-8](https://doi.org/10.1016/0043-1648(82)90342-8).
- Mortara, G., Mangiola, A. and Ghionna, V.N. (2007), "Cyclic shear stress degradation and post-cyclic behaviour from sand-steel interface direct shear tests", *Can. Geotech. J.*, **44**(7), 739-752. <https://doi.org/10.1139/t07-019>.
- Mu, W., Li, L., Yang, T., Yu, G. and Han, Y. (2019), "Numerical investigation on a grouting mechanism with slurry-rock coupling and shear displacement in a single rough fracture", *B. Eng. Geol. Environ.*, **78**(8), 6159-6177. <https://doi.org/10.1007/s10064-019-01535-w>.
- Nayak, P.R. (1973), "Some aspects of surface roughness measurement", *Wear*, **26**(2), 165-174. [https://doi.org/10.1016/0043-1648\(73\)90132-4](https://doi.org/10.1016/0043-1648(73)90132-4).
- Saberi, M., Annan, C.D. and Konrad, J.M. (2018), "A unified constitutive model for simulating stress-path dependency of sandy and gravelly soil-structure interfaces", *Int. J. Non-Linear Mech.*, **102**, 1-13. <https://doi.org/10.1016/j.ijnonlinmec.2018.03.001>.
- Saberi, M., Annan, C.D. and Konrad, J.M. (2018), "On the mechanics and modeling of interfaces between granular soils and structural materials", *Arch. Civ. Mech. Eng.*, **18**, 1562-1579. <https://doi.org/10.1016/j.acme.2018.06.003>.
- Saberi, M., Annan, C.D. and Konrad, J.M. (2019), "Implementation of a soil-structure interface constitutive model for application in geo-structures", *Soil Dyn. Earth Eng.*, **116**, 714-731. <https://doi.org/10.1016/j.soildyn.2018.11.001>.
- Saberi, M., Annan, C.D., Konrad, J.M. and Lashkari, A. (2016), "A critical state two-surface plasticity model for gravelly soil-

- structure interfaces under monotonic and cyclic loading”, *Comput. Geotech.*, **80**, 71-82.
<https://doi.org/10.1016/j.compgeo.2016.06.011>.
- Samanta, M., Punetha, P. and Sharma, M. (2018), “Effect of roughness on interface shear behavior of sand with steel and concrete surface”, *Geomech. Eng.*, **14**(4), 387-398.
<https://doi.org/10.12989/gae.2018.14.4.387>.
- Sayles, R.S. and Thomas, T.R. (1977), “The spatial representation of surface roughness by means of the structure function: A practical alternative to correlation”, *Wear*, **42**(2), 263-276.
[https://doi.org/10.1016/0043-1648\(77\)90057-6](https://doi.org/10.1016/0043-1648(77)90057-6).
- Su, L., Zhou, W., Chen, W. and Jie, X. (2018), “Effects of relative roughness and mean particle size on the shear strength of sand-steel interface”, *Measurement*, **122**, 339-346.
<https://doi.org/10.1016/j.measurement.2018.03.003>.
- Thomas, T.R. (1981), “Characterization of surface roughness”, *Precision Eng.*, **3**(2), 97-104.
[https://doi.org/10.1016/0141-6359\(81\)90043-X](https://doi.org/10.1016/0141-6359(81)90043-X).
- Tse, R. (1979), “Estimating joint roughness coefficients”, *Int. J. Rock Mech. Min. Sci. Geomech. Abstr.*, **16**(5), 303-307.
[https://doi.org/10.1016/0148-9062\(79\)90241-9](https://doi.org/10.1016/0148-9062(79)90241-9).
- Xiao, S., Suleiman, M.T. and McCartney, J.S. (2014), “Shear behavior of silty soil and soil-structure interface under temperature effects”, *Proceedings of the Geo-Congress 2014*, Atlanta, Georgia, U.S.A., February.
- Yazdani, S., Helwany, S. and Olgun, G. (2019), “Influence of temperature on soil-pile interface shear strength”, *Geomech. Energy Environ.*, **18**, 69-78.
<https://doi.org/10.1016/j.gete.2018.08.001>.
- Zhang, G. and Zhang, J. (2006), “Monotonic and cyclic tests of interface between structure and gravelly soil”, *Soils Found.*, **46**(4), 505-518. <https://doi.org/10.3208/sandf.46.505>.
- Zhang, G. and Zhang, J. (2009), “Constitutive rules of cyclic behavior of interface between structure and gravelly soil”, *Mech. Mater.*, **41**(1), 48-59.
<https://doi.org/10.1016/j.mechmat.2008.08.003>.
- Zhang, G. and Zhang, J. (2009), “State of the art: Mechanical behavior of soil-structure interface”, *Prog. Nat. Sci.*, **19**(10), 1187-1196. <https://doi.org/10.1016/j.pnsc.2008.09.012>.
- Zhang, G., Liang, D. and Zhang, J. (2006), “Image analysis measurement of soil particle movement during a soil-structure interface test”, *Comput. Geotech.*, **33**, 248-259.
<https://doi.org/10.1016/j.compgeo.2006.05.003>.
- Zhang, J., Hu, R. and Wang, X. (2017), “Effects of shear rate and effective shear area on shear strength of rock-soil aggregate in large-scale direct shear tests”, *J. Railway Sci. Eng.*, **14** (5), 971-979.
- Zhang, L.L. and Wang, X.J. (2017), “Correction of the shear area and error analysis in direct shear test”, *Mech. Eng.*, **39**(5), 468-471.
- Zhao, L., Yang, P., Zhang, L. and Wang, J. (2017), “Cyclic direct shear behaviors of an artificial frozen soil-structure interface under constant normal stress and sub-zero temperature”, *Cold Reg. Sci. Technol.*, **133**, 70-81.
<https://doi.org/10.1016/j.coldregions.2016.10.011>.